European Journal of Radiology 115 (2019) 1–9

Contents lists available at ScienceDirect

European Journal of Radiology

journal homepage: www.elsevier.com/locate/ejrad

Research article

Assessment of tumor heterogeneity: Differentiation of periampullary neoplasms based on CT whole-lesion histogram analysis

Jingyu Lu[a,1], Daoyu Hu[a,1], Hao Tang[a], Xuemei Hu[a], Yaqi Shen[a], Zhen Li[a], Yang Peng[a,*], Ihab Kamel[b]

[a] Department of Radiology, Tongji Hospital, Tongji Medical College, Huazhong University of Science and Technology, 1095 Jiefang Avenue, Wuhan, Hubei, 430030, PR China

[b] Russell H. Morgan Department of Radiology and Radiological Science, The Johns Hopkins Medical Institutions, Baltimore, Maryland, USA

ARTICLE INFO

Keywords:
Ampulla of Vater
Duodenal adenocarcinoma
Pancreatic ductal adenocarcinoma
Gastrointestinal stromal tumor
Multidetector computed tomography

ABSTRACT

Purpose: To investigate the utility of whole-lesion histogram analysis from multidetector computed tomography (MDCT) for discrimination of duodenal adenocarcinoma (DAC), pancreatic ductal adenocarcinoma (PDAC) and gastrointestinal stromal tumor (GIST) around the periampullary area.

Materials and methods: 171 patients suspicious of periampullary tumors were examined by MDCT (arterial and venous phases) and treated with surgery. A total of 74 patients were finally included in this retrospective study (26 DACs, 20 PDACs, and 28 GISTs). The interobserver agreement was evaluated by intra-class correlation coefficient (ICC) test between two radiologists. Volumetric histogram analysis based on CT Kinetics software was performed on enhanced MDCT images that recorded different histogram parameters of arterial and venous phases, including mean, median, 10th, 25th, 75th, and 90th percentiles, as well as skewness, kurtosis and entropy. The extracted histogram parameters were compared between DAC, PDAC and GIST respectively by Mann-Whitney U tests with Bonferroni corrections. Receiver operating characteristic (ROC) curve analysis was used to determine the diagnostic ability of each significant parameter and the area under the curve (AUC) was calculated.

Results: The whole-lesion CT histogram analysis demonstrated significant differences between DAC, PDAC, and GIST with different histogram features on both arterial and venous phase scans (all $P < 0.05$). In the ROC analysis, the 90th percentile of venous phase demonstrated the highest AUC of 0.854 ($P < 0.001$) for discriminating DAC from PDAC. Excellent discriminators of periampullary tumors were noted among the histogram features, namely the 90th percentile of arterial phase, which demonstrated AUCs of 0.809 and 0.936 ($P < 0.001$) respectively for distinguishing DAC and PDAC from GIST.

Conclusion: The whole-lesion CT histogram analysis could be useful for differential diagnosis of DAC, PDAC and GIST arising from the periampullary area. Further assessment is warranted to investigate the clinical role of histogram analysis based on MDCT.

1. Introduction

The periampullary tumor refers to a mass located around the region of the ampulla of Vater, which includes ampulla of Vater itself, the head and uncinate process of pancreas, the distal part of common bile duct, and parts of duodenum. The periampullary adenocarcinoma, which is rarely seen, accounts for 6% of periampullary tumors and only 0.2% of all gastrointestinal tumors [1–3]. The periampullary adenocarcinomas are usually divided into intestinal and pancreatobiliary subtypes according to a widely accepted classification [4–6]. The pancreatic ductal adenocarcinoma (PDAC) and duodenal adenocarcinoma (DAC) are representatives of pancreatobiliary and intestinal subtypes. On the other

Abbreviations: MDCT, multidetector computed tomography; DAC, duodenal adenocarcinoma; PDAC, pancreatic ductal adenocarcinoma; GIST, gastrointestinal stromal tumor; MRCP, magnetic resonance cholangiopancreatography; DWI, diffusion-weighted imaging; ICC, intra-class correlation coefficient; ROC, receiver operating characteristic curve; AUC, area under the curve; AP, arterial phase; VP, venous phase; ROI, region-of-interest; VOI, volume-of-interest

* Corresponding author.

E-mail addresses: luugbas@126.com (J. Lu), daoyuhu@hust.edu.cn (D. Hu), haotangtjh@163.com (H. Tang), mayjuly3720@163.com (X. Hu), yqshen@hust.edu.cn (Y. Shen), zhenli@hust.edu.cn (Z. Li), peterpengyang@126.com (Y. Peng), ikamel@jhmi.edu (I. Kamel).

[1] Drs. Lu and Hu contributed equally as first authors to this work.

https://doi.org/10.1016/j.ejrad.2019.03.021
Received 18 October 2018; Received in revised form 25 March 2019; Accepted 26 March 2019
0720-048X/ © 2019 Elsevier B.V. All rights reserved.

hand, the gastrointestinal stromal tumor (GIST), the most common mesenchymal tumor of gastrointestinal tract, often occurs in small intestine and stomach, with rare occurrence in the duodenum [7,8]. In the periampullary region, PDAC, DAC and GIST make up approximately 3%, 0.4% and 2% of gastrointestinal malignancies respectively [7,9,10].

Previous studies showed that these two subtypes of adenocarcinomas and GIST differed in treatment planning and prognosis [7,11–13]. The major treatment for early stage of periampullary tumor is radical surgery resection with tumor-free margin. It was reported that only 10–15% of PDAC patients would potentially have curative surgery (pancreaticoduodenectomy) without relapse of disease [14]. But periampullary DAC and GIST could be completely removed by surgery. Regarding prognosis, PDAC shows five-year survival rate of less than 4% [15]; DAC shows five-year survival rate of 29.0–55.9% [13,16,17] and GIST shows five-year survival rate of 89.1%(8). Thus, the accurate preoperative imaging discrimination of periampullary tumors is essential to optimize treatment plans and patient outcome.

Computed tomography (CT) is the most commonly used non-invasive cross-sectional imaging modality in the evaluation of periampullary lesions [18]. Although CT and MRI analyses of masses arising from periampullary region were reported by several studies [19–21], discrimination between DAC, PDAC and GIST remains challenging because of anatomical complexity of the periampullary area. Various techniques using CT and MR imaging have been utilized to render investigation of the ampulla region possible, including MDCT (multidetector computed tomography), MRCP (MR cholangiopancreatography), and DWI (diffusion-weighted imaging) [19,21,22]. MDCT has comparatively good spatial resolution; meanwhile, the distribution and intensity of pixels in corresponding CT images could reflect the biological and physiological properties of studying objects attenuating the X-ray beam [23,24]. Recently, many findings showed that CT-derived tumor gray-level heterogeneity was associated with pathological features of different tumor types, tumor treatment response to treatment, and prognosis [25–29]. CT histogram analysis is a new non-invasive and quantitative method by computer-assisted assessment of tumor heterogeneity, which is related to the distribution and relationship of pixel or voxel gray levels in corresponding CT images. Tumors of periampullary area are heterogeneous on histopathological levels, characterized by intratumoral spatial complexity in angiogenesis, cellularity, extravascular extracellular matrix, and necrosis. Tumors with higher heterogeneity are often associated with poorer prognosis due to innate aggressive nature of tumor itself. Compared to the randomized sampling and biopsy, the whole-lesion histogram method could better evaluate tumor heterogeneity at almost full extent of tissue variations within tumors. Besides, this approach is independent of subjective visual interpretation. Moreover, the whole volume histogram analysis, covering the entire lesion, could capture more comprehensive information about tumor heterogeneity than single-slice method. The utility of whole volume approach decreases sampling errors and enhances reliability and reproducibility of quantitative volume analysis. To date, no investigation has been reported to distinguish between DAC, PDAC and GIST using whole-lesion CT histogram analysis. The purpose of this study is to evaluate the diagnostic performance of CT volumetric histogram analysis in differentiation of DAC, PDAC and GIST.

2. Materials and methods

2.1. Patients

Institutional Ethics Review Board approval was obtained, and informed consent was waived for this retrospective study. Retrospective review of our institution's imaging database identified 171 patients with suspected periampullary tumors who underwent abdominal dual-phase enhanced MDCT between March 2014 and June 2017. The identification of eligible patients was based on the selection report containing chosen criteria. Meanwhile, the selection process was performed by another radiologist, who was different from the radiologists, who performed CT image analysis. The inclusion criteria were as follows :(a) preoperative MDCT examination was conducted 2 weeks before surgery; (b) the tumor was located in the ampullary region; (c) patients had pathologically proven DAC, PDAC or GIST;(d) no invasive examination or treatment was performed before surgery. The exclusion criteria were as follows: (a) tumors were not located in ampullary areas (n = 71); (b) the pathological results of ampullary tumors were not adenocarcinoma or stromal tumors (n = 3); (c) patients received invasive examination or treatment before surgery (n = 10). All the studied patients received preoperative MDCT 2 weeks before surgery. 84 patients were excluded according to the above exclusion criteria. 4 patients were excluded because no obvious masses were recognized and nine patients were excluded because of poor image quality. The final cohort was consisted of 74 patients (33 women, 41 men; mean age, 53 years; age range, 26–75 years) in our study (Fig. 1).

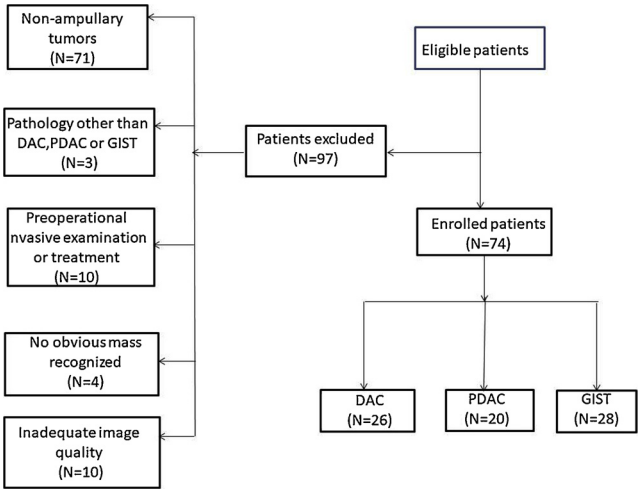

Fig. 1. Flowchart of the study population.

2.2. CT examination

All CT examinations were performed using a 64-channel multi-detector CT scanner (Discovery 750, GE healthcare, United States). All patients underwent contrast enhanced CT scan, and the scan range covered the whole abdomen (from the top of the diaphragm to the lower edge of the pubic symphysis). Patients were informed to hold their breath at the end of deep inspiration during imaging scan. For special circumstances, patients were allowed to breath gently to reduce respiratory movement if they cannot tolerate breath-holding. For each patient, the iopromide (Ultravist 370, 370 mg/ mL, Bayer Schering Pharma, Berlin, Germany) was administered in an antecubital vein with a power injector (Stellant, Medrad, CO, USA) at a dose of 1.5 mL per kilogram of body weight at a rate of 3.5 mL/sec, followed by 20 mL saline solution. The initiation of arterial phase was performed 5–8 s after calculated CT value reached 120HU attenuation at the descending aorta by utility of a bolus-tracking method. The imaging scan time delay for arterial phase (AP) and venous phase (VP) were 25–30 s and 55–60 s respectively. The venous phase imaging was achieved 25–30 s after the completion of arterial phase imaging. The CT scanning parameters were as follows: tube voltage, 100 kV; tube current, 120–250 mA; beam collimation, 64 × 0.625; single turn of tube rotation time, 0.6 s; detector pitch, 0.984. Images were exhibited in axial plane with section thickness of 2.5–5 mm, and multi-planar reformatted images with slice thickness of 1 mm were available for clinical interpretation. The multi-planar reformatted images referred to images,

which were reconstructed in axial, coronal and sagittal planes. The comparatively thin-sliced reconstructed images could provide better viewing of different periampullary neoplasms.

2.3. Quantitative histogram analysis

Patient-identifying information was removed from each CT image for the 74 patients studied for histogram analysis, which is a first-order texture analysis by using histogram methods without filters. All raw data were transferred to a PC and processed with commercially-available software CT Kinetics (GE Healthcare, China). Two radiologists with 6 and 8 years of experience in abdominal imaging, reviewed all the CT images independently. They were blinded to the patients' clinical and pathologic information. Each image was manually contoured by the two radiologists respectively to define the outer margin of lesion, and the contour was saved as ROI for further histogram analysis. Region-of-interest (ROI) was drawn along the outer margin of the whole lesion on continuous slices and finally each layer of ROI merged to get the 3D volume-of-interest (3D VOI). The highest and lowest slices of CT images related to lesions were excluded to avoid partial volume effects. Attention was paid to cover only the whole lesion and avoid the peritumoral blood vessels, normal intestinal wall, intestinal gas, intra-abdominal adipose tissue, adjacent organs, tumor necrosis and calcification. The drawing of margin along the lesion was performed slightly within the lesion borders to eschew the volume averaging from surrounding normal intestinal wall or other periampullary structures. The two radiologists performed the ROI delineation independently to assess the interobserver agreement in ROI determination, which may influence the obtaining of histogram parameters. The volumetric histogram was automatically calculated by CT Kinetics software. The mean, median, 10^{th}, 25th, 75th, 90th percentiles of CT attenuation value, kurtosis, skewness and entropy of arterial phase and venous phase were obtained.

2.4. Statistical analysis

Patient age and tumor size of DAC, PDAC and GIST groups were compared by the independent student *t*-test Shapiro-Wilk tests were performed to check whether the extracted features for histogram parameters from CT images were normally distributed before subsequent analysis. If normally distributed, the value of each histogram parameter was compared between DAC, PDAC and GIST respectively by student t or by Mann-Whitney U test if not normally distributed. Bonferroni corrections were applied for histogram features to account for the multiple comparisons that were made between different groups. Receiver operating characteristics (ROC) analysis was utilized to determine the potential diagnostic performance for differentiation of these periampullary tumors. The area under the ROC curve (AUC) with 95% confidence intervals (95% CI) was calculated for each histogram parameter. Interobserver agreement was performed by the intraclass correlation coefficient (ICC) test (0.00–0.20, poor agreement; 0.21–0.40, fair agreement; 0.41–0.60, moderate agreement; 0.61-0.80, good agreement; 0.81–1.00, excellent agreement). Statistical analyses were performed using the Statistical Package for the Social Sciences (SPSS, version 19.0, IBM, Armonk, NY, USA) and MedCalc (MedCalc software, version 12.7.0.0, Mariakerke, Belgium). Differences with P value less than 0.05 were considered statistically significant.

3. Results

3.1. Patient characteristics

The histopathological results revealed 26 DACs, 20 PDACs and 28 GISTs. No significant difference was found in age between DAC (mean ± SD, 58.3 ± 8.9 years), PDAC (58.9 ± 7.4 years) and GIST (55.0 ± 9.3 years) groups (DAC vs. PDAC, P = 0.810; DAC vs. GIST, P = 0.209; PDAC vs. GIST, P = 0.089). GISTs (55.0 ± 9.3 mm) were larger than DACs (19.2 ± 6.7 mm) and PDACs (22.4 ± 5.0 mm) (GIST vs. DAC, P < 0.0001; GIST vs. PDAC, P < 0.0001). There was no significant difference in tumor size between DAC and PDAC (P = 0.070). The clinical characteristics and histopathological findings are presented in Table 1.

Table 1
Patient Characteristics.

Characteristics	DAC (n = 26)	PDAC (n = 20)	GIST (n = 28)
Sex			
Male	18	12	11
Female	8	8	17
Patient age (y)[§]	58.3 ± 8.9	58.9 ± 7.4	55.0 ± 9.3
Tumor size (mm)[☆]	19.2 ± 6.7	22.4 ± 5.0	52.7 ± 39.7
Histological grade[★]			
well-differentiated	4	3	17
moderately-differentiated	19	16	2
poorly-differentiated	3	1	9

Note: ————.

[§] Data are mean age ± standard deviation. There was no significant difference between DAC, PDAC and GIST groups (DAC vs. PDAC, P = 0.810; DAC vs. GIST, P = 0.209; PDAC vs. GIST, P = 0.089).

[☆] Data are mean tumor size ± standard deviation. The mean tumor size was significantly larger in the GIST group (GIST vs. DAC, P < 0.0001; GIST vs. PDAC, P < 0.0001). There was no significant difference between DAC and PDAC group (P = 0.070).

[★] In the group of GISTs, 'well' represented 'low risk', 'moderately' represented 'intermediate risk', and 'poorly' represented 'high risk'.

3.2. Interobserver agreement

Overall, the interoberver agreement between two readers was excellent for the whole- tumor volume histogram metrics of mean, median, 10th, 25th, 75th, 90th percentile, skewness, kurtosis, and entropy (ICCs ranged from0.936 to 0.999). The ICC values for each histogram-based parameter are shown in Table 2.

3.3. Comparison of CT attenuation value for histogram parameters between DAC, PDAC and GIST

In both arterial and venous phases, mean, median, 10th, 25th, 75th and 90th percentiles of CT attenuation value of PDAC were the lowest (56.05 ± 11.99, 55.38 ± 10.59, 29.61 ± 13.12, 41.91 ± 11.60, 68.82 ± 10.61, 81.19 ± 11.86 for arterial phase; 64.38 ± 20.70, 63.34 ± 16.95, 35.32 ± 17.77, 48.65 ± 17.17, 77.71 ± 17.44, 92.69 ± 25.59 for venous phase) among these three types of tumors, while GISTs achieved the highest CT attenuation value (91.61 ± 21.70, 90.92 ± 27.87, 55.10 ± 26.88, 72.11 ± 27.13, 110.52 ± 28.56, 128.89 ± 29.86 for arterial phase; 94.79 ± 24.89, 94.73 ± 25.44, 60.37 ± 27.03, 77.13 ± 26.31, 107.30 ± 18.12, 128.71 ± 24.97 for venous phase) (Fig. 2, Table 3). There were

Table 2
Interobserver agreement for whole-tumor CT histogram parameters.

Parameter	Intraclass correlation coefficient	95% confidence interval
Mean	0.996	0.994–0.997
Median	0.996	0.994–0.997
10^{th} percentile	0.994	0.991–0.995
25^{th} percentile	0.995	0.993–0.996
75^{th} percentile	0.996	0.995–0.997
90^{th} percentile	0.996	0.995–0.997
Skewness	0.996	0.995–0.997
Kurtosis	0.999	0.999–1.000
Entropy	0.936	0.912–0.954

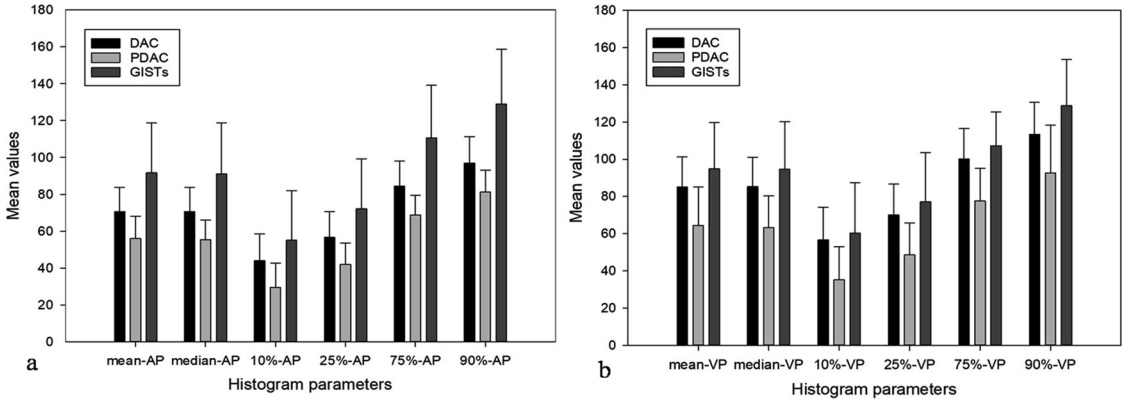

Fig. 2. Bar charts demonstrated the comparison of CT histogram parameters for arterial phase (AP, a) and venous phase (VP, b) between duodenal adenocarcinoma (DAC), pancreatic duct adenocarcinoma (PDAC) and duodenal gastrointestinal stromal tumors (GISTs).

significant differences for mean, median, 10th, 25th, 75th and 90th percentiles of CT value between DAC and PDAC, PDAC and GIST ($P < 0.005$) in both arterial and venous phases. In the comparison of DAC and GIST, the differences for mean, median, 25th, 75th and 90th percentiles of CT value in arterial phase were significant ($P = 0.002$, $P = 0.004$, $P = 0.033$, $P = 0.000$, $P = 0.000$ respectively). In venous phase, only 90th percentile of CT value was found to be significantly different between DAC and GIST (113.26 ± 17.43 vs. 128.71 ± 17.43, $P = 0.015$). As for analysis of skewness, kurtosis and entropy, there was significant difference for skewness in arterial phase between DAC and GIST (-0.02 ± 0.09 vs. 0.17 ± 0.33, $P = 0.015$). No other significant differences occurred between the three types of peri-ampullary tumors.

3.4. Diagnostic performance of histogram parameters for differentiating DAC, PDAC and GIST

In the ROC analysis, the 90th percentile of venous phase generated

Table 3
Comparison of CT histogram parameters for differentiation of DAC, PDAC and GIST.

Parameter	Arterial phase						Venous phase					
	DAC	P§	PDAC	P☆	GIST	P★	DAC	P§	PDAC	P☆	GIST	P★
Mean	70.58 ± 13.25	**0.001**	56.05 ± 11.99	**0.000**	91.61 ± 27.10	**0.002**	85.19 ± 16.06	**0.001**	64.38 ± 20.70	**0.000**	94.79 ± 24.89	0.098
Median	70.60 ± 13.20	**0.000**	55.38 ± 10.59	**0.000**	90.92 ± 27.87	**0.004**	85.23 ± 15.90	**0.000**	63.34 ± 16.95	**0.000**	94.73 ± 25.44	0.281
10^{th}	44.02 ± 14.61	**0.000**	29.61 ± 13.12	**0.000**	55.10 ± 26.88	**0.004**	56.70 ± 17.49	**0.001**	35.32 ± 17.77	**0.001**	60.37 ± 27.03	0.912
25^{th}	56.70 ± 13.85	**0.001**	41.91 ± 11.60	**0.000**	72.11 ± 27.13	**0.033**	70.16 ± 16.53	**0.000**	48.65 ± 17.17	**0.000**	77.13 ± 26.31	0.572
75^{th}	84.53 ± 13.48	**0.000**	68.82 ± 10.61	**0.000**	110.52 ± 28.56	**0.000**	100.13 ± 16.31	**0.000**	77.71 ± 17.44	**0.000**	107.30 ± 18.12	0.133
90^{th}	96.82 ± 14.40	**0.001**	81.19 ± 11.86	**0.000**	128.89 ± 29.86	**0.000**	113.26 ± 17.43	**0.002**	92.69 ± 25.59	**0.000**	128.71 ± 24.97	**0.015**
SD	20.76 ± 4.48	0.422	22.94 ± 14.51	**0.026**	28.97 ± 6.97	**0.001**	22.56 ± 5.02	0.330	25.56 ± 19.59	0.728	26.71 ± 6.57	0.152
Skewness	−0.02 ± 0.09	0.641	0.32 ± 1.39	0.957	0.17 ± 0.33	**0.015**	−0.01 ± 0.15	0.255	0.19 ± 1.07	0.117	−0.08 ± 0.30	0.653
Kurtosis	3.06 ± 0.28	0.688	5.52 ± 10.82	0.755	3.31 ± 0.51	0.866	3.05 ± 0.21	0.708	4.44 ± 6.33	0.749	3.14 ± 0.46	0.709
Entropy	6.23 ± 0.30	0.060	5.90 ± 0.92	0.962	5.88 ± 0.49	0.069	6.15 ± 0.36	0.912	6.00 ± 1.04	1.000	6.02 ± 0.44	0.599

Note: ————.
DAC: duodenal adenocarcinoma; PDAC: pancreatic ductal adenocarcinoma; GIST: gastrointestinal stromal tumor.
Values are presented as Mean ± standard deviations. SD = standard deviation.
10 th, 25th, 75th and 90th represented 10th percentile, 25th percentile, 75th percentile and 90th percentile of CT attenuation value respectively.
§ The comparison of histogram parameters between DAC and PDAC.
☆ The comparison of histogram parameters between PDAC and GIST.
★ The comparison of histogram parameters between GIST and DAC.

Table 4
Diagnostic performance of histogram parameters for differentiation of DAC, PDAC and GIST.

AP	DAC vs. PDAC				DAC vs. GIST				PDAC vs. GIST			
Parameter	AUC	cutoff	Sensitivity (%)	specificity (%)	AUC	cutoff	sensitivity (%)	specificity (%)	AUC	cutoff	sensitivity (%)	specificity (%)
Mean	0.821	63.63	73.1	85.0	0.734	92.82	57.1	100.0	0.880	63.35	85.7	85.0
Median	0.835	63.68	73.1	85.0	0.714	93.05	57.1	100.0	0.868	64.62	82.1	85.0
10th	0.754	44.48	53.8	100.0					0.809	44.17	64.3	100.0
25th	0.794	57.51	53.8	100.0	0.694	78.43	50.0	100.0	0.837	51.32	82.1	85.0
75th	0.831	74.38	88.5	75.0	0.766	109.77	57.1	100.0	0.909	80.47	85.7	85.0
90th	0.804	85.75	88.5	75.0	0.809	123.51	64.3	100.0	0.936	95.87	85.7	90.0
Skewness					0.799	0.08	71.4	92.3				
Mean	0.829	75.01	76.9	85.0					0.837	86.49	64.3	95.0
Median	0.835	75.24	76.9	85.0					0.839	86.74	64.3	95.0
10th	0.829	39.33	92.3	65.0					0.768	55.46	57.1	95.0
25th	0.838	62.76	73.1	85.0					0.805	66.31	67.9	90.0
75th	0.850	84.31	84.6	80.0					0.896	90.27	85.7	85.0
90th	0.854	94.46	92.3	80.0	0.695	112.88	78.6	61.5	0.895	96.92	89.3	80.0

Note: ————.
10 th, 25th, 75th and 90th represented 10th percentile, 25th percentile, 75th percentile and 90th percentile of CT attenuation value respectively.
The blank spaces indicated corresponding parameters were not significant in differentiation of periampullary tumors.
AP = arterial phase, VP = venous phase.

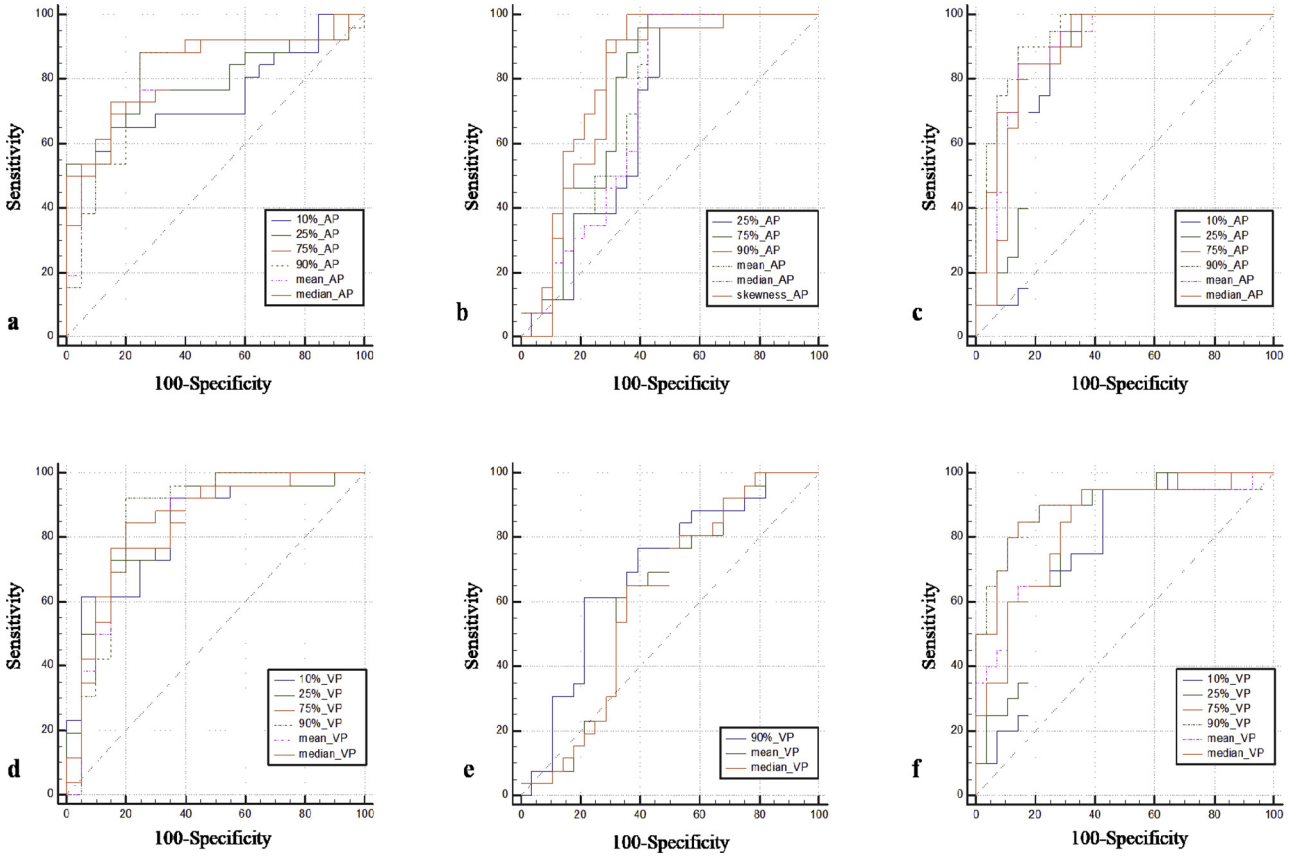

Fig. 3. ROC curves for whole-tumor histogram parameters in differentiating DAC from PDAC (**a, d**), DAC from GISTs (**b, e**) and PDAC from GISTs (**c, f**) at arterial phase (**a, b, c**) and venous phase (**d, e, f**) of enhanced CT scan.

the highest AUC (0.854; 95%CI, 0.726-0.981; P < 0.001) for differentiating DAC from PDAC with sensitivity of 92.3% and specificity of 80%. The 90th percentile of arterial phase achieved the highest AUC (0.809; 95%CI, 0.687–0.931; P < 0.001) for discrimination of DAC from duodenal GIST with sensitivity of 100% and specificity of 64%. As for differentiation of PDAC from GIST, the 90th percentile of arterial phase had the highest AUC up to 0.936 (95%CI, 0.871–1.000; P < 0.001), with sensitivity of 90% and specificity of 86%. The ROC curves analysis and diagnostic performance are provided in Table 4 and Fig. 3. Representative images of DAC, PDAC and GIST are shown in Figs. 4–6 respectively.

4. Discussion

This study focused on the role of histogram analysis based on MDCT imaging technique for differentiation of DAC, PDAC and GIST, which occurred in periampullary areas. The results of this study indicated a wide range of AUCs for discrimination of above three periamullary

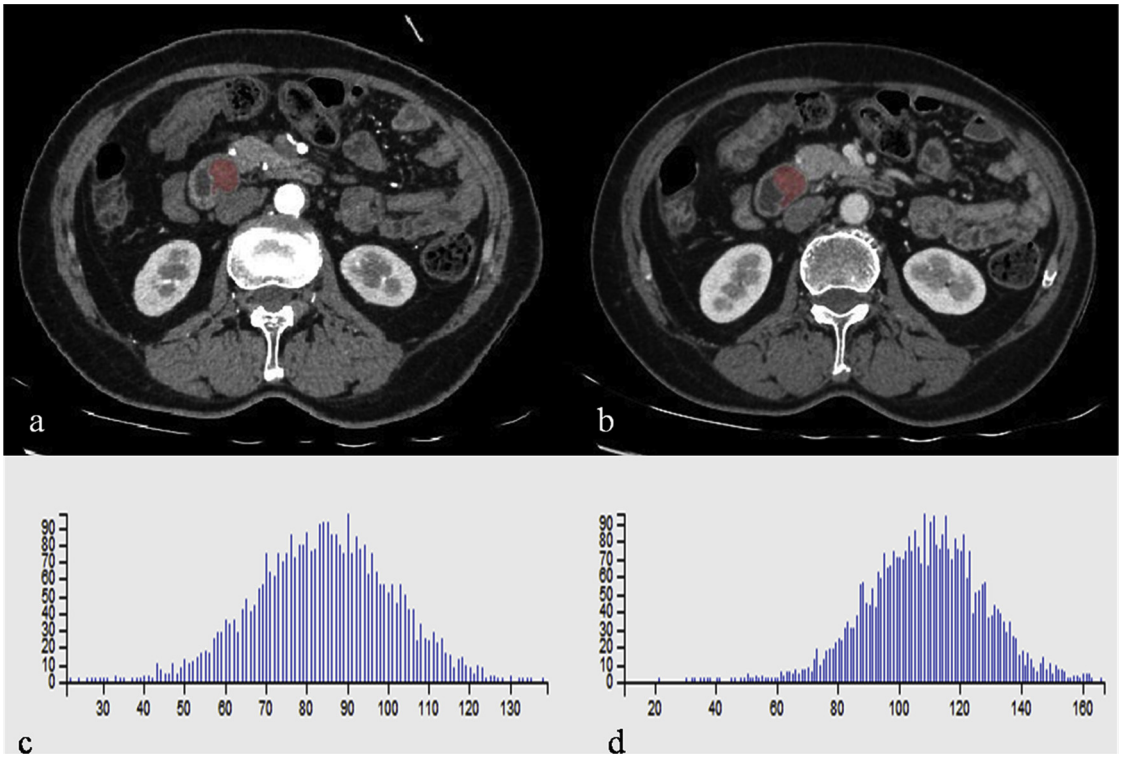

Fig. 4. A 62-year-old female with DAC. The tumor region of interest (ROI) was localized on axial CT images at arterial phase (**a**) and venous phase (**b**). CT whole-tumor histograms at arterial phase (mean_AP, 88.582HU; skewness_AP, 0.017; kurtosis_AP, 3.021; entropy_AP, 6.376) (**c**) and venous phase (mean_VP, 117.987HU; skewness_VP, 0.279; kurtosis_VP, 2.962; entropy_VP, 6.353) (**d**) were shown.

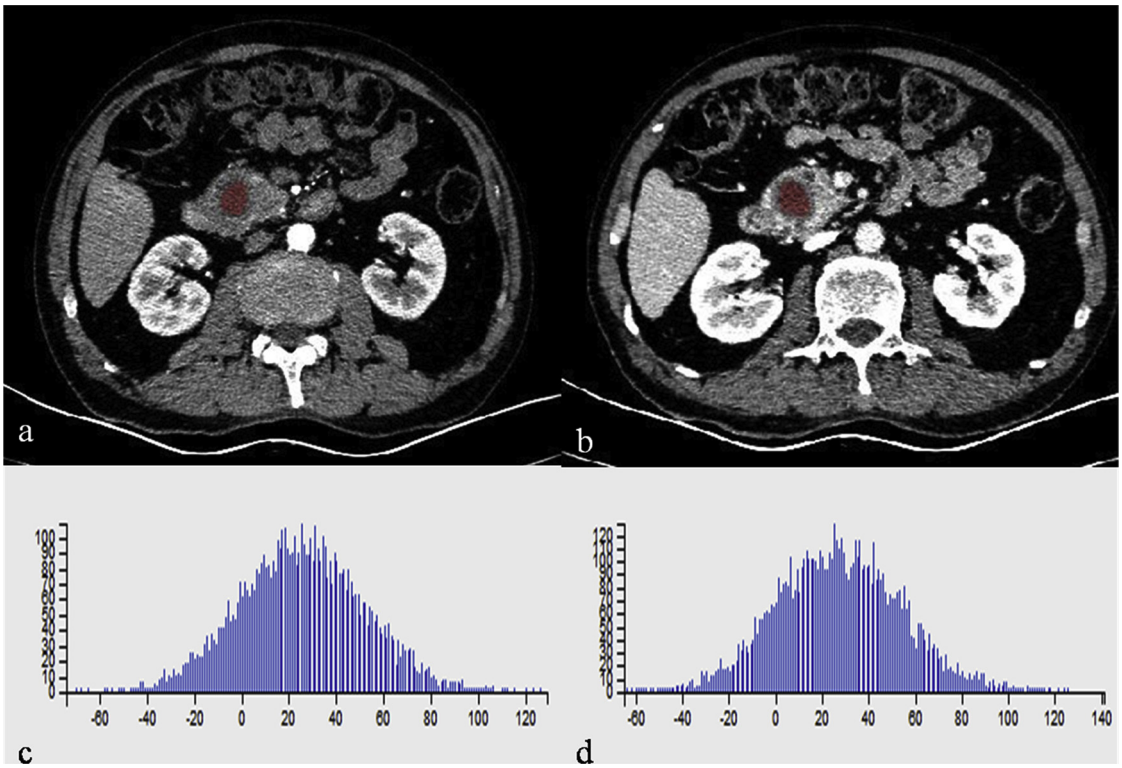

Fig. 5. A 59-year-old male with PDAC. The tumor region of interest (ROI) was localized on axial CT images at arterial phase (**a**) and venous phase (**b**). CT whole-tumor histograms at arterial phase (mean_AP, 25.117HU; skewness_AP, 0.115; kurtosis_AP, 3.099; entropy_AP, 6.069) (**c**) and venous phase (mean_VP, 26.727HU; skewness_VP, 0.112; kurtosis_VP, 3.171; entropy_VP, 6.077) (**d**) were shown.

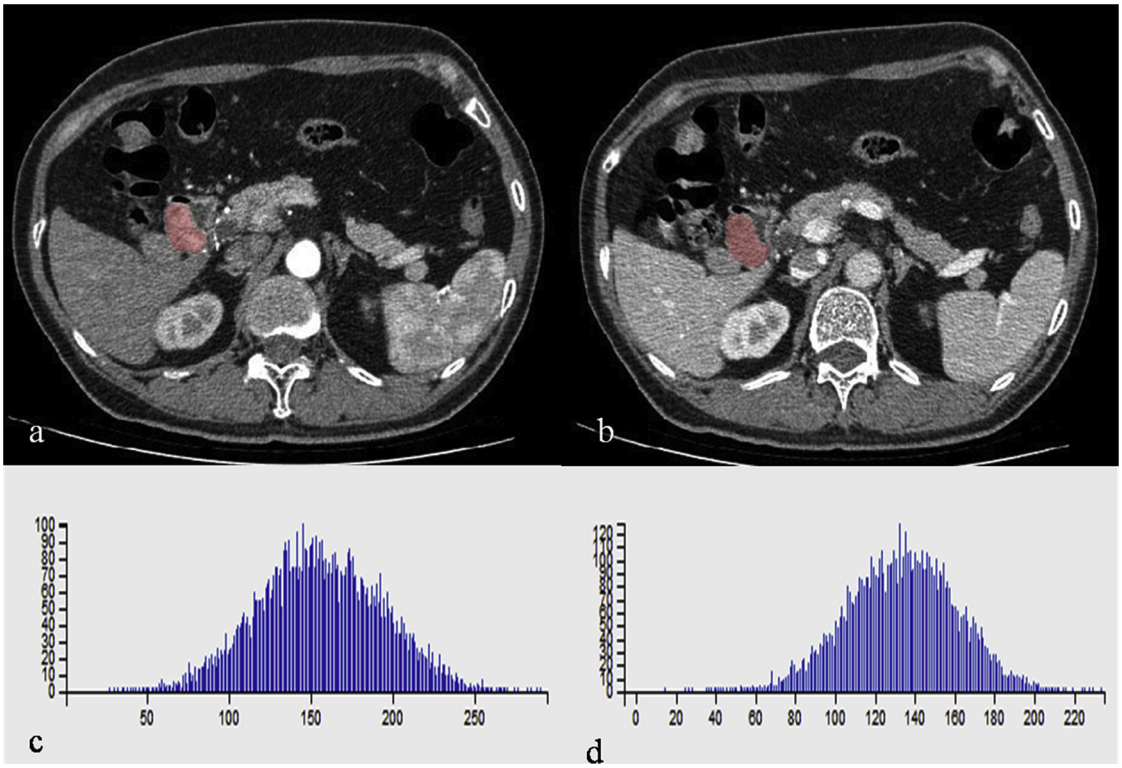

Fig. 6. A 60-year-old female with duodenal GIST.The tumor region of interest (ROI) was localized on axial CT images at arterial phase (**a**) and venous phase (**b**). CT whole-tumor histograms at arterial phase (mean_AP, 155.150HU; skewness_AP, 0.019; kurtosis_AP, 3.000; entropy_AP, 6.205) (**c**) and venous phase (mean_VP, 133.262HU; skewness_VP, –0.096; kurtosis_VP, 3.081; entropy_VP, 6.147) (**d**) were shown.

tumors, noting that CT-based histogram features could provide valuable information for differential diagnosis.

In our study, the interobserver agreement between two abdominal radiologists was excellent for all histogram parameters. The excellent interobserver variability confirmed comparatively good reliability and reproducibility of volumetric CT histogram analysis.

CT histogram analysis is a form of computer-assisted CT image processing tool by extracting related histogram features objectively in a quantitative manner, which allows for mathematical calculation of pixel level distribution in different kinds of tumors. This technique could capture information about subtle differences, which cannot be detected with naked eyes. The derived histogram features could be correlated with tumor biological behaviors by this image processing tool, which would have clinical implications for tumor treatment and prognosis.

Significant differences were found in various histogram features, which were used to differentiate between DAC, PDAC and GIST. The possible explanation for the difference of the above three tumors could be associated with tumor heterogeneity, which has been reported to relate to tumor malignancy [27]. Tumor heterogeneity was mainly influenced by tumor neovascularization, tumor cellular density, microcirculation structure transformation, and other pathological components in tumor tissues. Increased heterogeneity in malignant tumors was often accompanied by tumor cell infiltration and abnormal tumor angiogenesis. To date, no investigations have been made to figure out the role of tumor heterogeneity derived from histogram features of CT images in distinguishing between DAC, PDAC and GIST in periampullary areas. There were several studies about CT histogram analysis demonstrating that heterogeneity was related to tumor biological behaviors and malignancy. In a study of 43 patients with two kinds of solid lung cancers (adenocarcinoma and squamous cell carcinoma), the final result indicated that CT histogram features were helpful for differentiation of solid lung adenocarcinoma from squamous cell carcinoma with adenocarcinoma having greater tumor heterogeneity [30]. In a study of 93 patients with 117 adrenal lesions, combined methods of CT histogram analysis and positron emission tomography indicated that histogram features and standard uptake value (SUV) differed significantly between benign adrenal masses and malignant ones with more heterogeneous tissue structures [31].

The histopathology characteristics of DAC, PDAC and GIST were different, and the variances of pathological features were demonstrated by corresponding histogram analysis. The histopathology- based tumor biological behaviors were closely associated with tumor heterogeneity. Previous studies showed that DAC, PDAC and GIST were presented with conspicuous structural and cellular heterogeneity, often with some coexisting pathological patterns [32–34]. The pathological feature of DAC is characterized by tumor cells which are pseudostratified tall columnar with oval or cigar-shaped nuclei and usually contain mucin. DAC is often consisted of well-tubular glands, solid nests and complicated cribriform areas, which are indistinctive to the colorectal cancer [35]. However, PDAC is presented in a different way, showing simple or branching glandular patterns of ductal structures with diverse differentiation degrees, accompanied by rich fibrous stroma. The tumor cells are arranged in a single layer with cuboidal or low- columnar type without pseudostratified nuclei and these cells differed from one to another in shape and size with round nuclei [35]. Moreover, the prominent histopathological traits of GIST are presented by rounded or spindle cells with rich and clear cytoplasm. The tumor cells are often displayed in packets or sheets, and they are inclined to grow in a perivascular pattern [36]. At a molecular level, the heterogeneity of periampullary tumors could also be reflected. For example, as for patients with PDAC and GIST, the up-regulation of FoxM1(Forkhead box M1), a very important transcription factor related to the expression of several genes, which were key to the aspects of tumor biological behaviors, could promote tumor growth and invasion of surrounding structures, leading to tumor progression and poorer prognosis [37,38]. Therefore, it could be hypothesized that the variations of tumor pathological components in DAC, PDAC and GIST could be pertinent to

the heterogeneity from histogram parameters based on MDCT, as was indicated in our study.

Our study was different from other studies focusing on the subjective analysis of MDCT findings on enhanced images to differentiate periampullary tumors [19,20] and the results of our study were influenced by the following factors. First, our study was based on the objective assessment of whole-lesion histogram analysis to make differential diagnosis. The CT images covering the entire tumor were analyzed instead of a single-slice CT image. This kind of computer-assisted method could extract more histogram features, representing more comprehensive information of tumor heterogeneity about diverse periampullary tumors. Second, our study was mainly concerned with CT enhanced images, and unenhanced CT images were not considered. Third, the histogram analysis could reflect the diversities of the underlying biological behaviors between various periampullary tumor types. It was reported that tumor heterogeneity could be better demonstrated on enhanced CT images, because tumor vascular supply played an important role in tumor heterogeneity [39]. Meanwhile, histogram features from biphasic enhanced CT images would also reflect the dynamic distribution of contrast media in the intracellular, extracellular and extravascular gap, which could indicate the biological behaviors of different periampullary tumors. Vascular permeability was mentioned in previous study [29] to explain the featured imaging manifestation of colorectal cancer on enhanced CT images. The findings in our study about the comparison of periampullary neoplasms could also be attributed to the effects of tumor vascular permeability. Higher vascular permeability (immature neovascularization) may be related to tumors with poor differentiation, and it may demonstrate higher tumor heterogeneity by histogram analysis. For instance, two studies found that higher vascularization formation and vascular permeability were associated with higher risk of metastasis in GIST with greater tumor heterogeneity [40,41]. Another study showed that more immature vascularization with higher vascular permeability was found in colorectal cancer with poor differentiation, leading to poorer prognosis [42].

There were some limitations in our study. First, it was a retrospective study with possible biases in patient selection. Only patients receiving surgical operations were included in this study, so the study objects may not reflect the entire spectrum of patients having DAC, PDAC and GIST of periampullary region. Second, the enrolled population was comparatively small, further study with larger number of patients was needed to enhance the reliability and reproducibility of this study. Third, there were other uncommon periampullary tumors, such as pancreatic neuroendocrine tumor (NET), solid pseudopapillary neoplasm (SPN), or distal common bile duct carcinoma, which were not included in our study. A more comprehensive population with different types of periampullary tumors was warranted to strengthen these initial findings.

In conclusion, the whole-lesion CT histogram analysis may act as promising, non-invasive diagnostic tool to differentiate the periampullary tumors (DAC, PDAC and GIST), but further studies are entailed before introduction of histogram analysis into the clinical workflow of the periampullary neoplasms.

Conflict of interest

Jingyu Lu, MD no conflict of interest.
Daoyu Hu, MD, PHD no conflict of interest.
Hao Tang, MD no conflict of interest.
Xuemei Hu, MD, PHD no conflict of interest.
Yaqi Shen, MD, PHD no conflict of interest.
Zhen Li, MD, PHD no conflict of interest.
Yang Peng, MD no conflict of interest.
Ihab Kamel, MD, PHD no conflict of interest.

Funding

This work was supported by the National Natural Science Foundation of China (No. 81801695, 81771801, 81701657, 81501447, 81571642) and the Fundamental Research Funds for the Central Universities (NO. 2017KFYXJJ126).

References

[1] J.T. Carter, J.P. Grenert, L. Rubenstein, L. Stewart, L.W. Way, Tumors of the ampulla of Vater: histopathologic classification and predictors of survival, J. Am. Coll. Surg. 207 (2008) 210–218.
[2] J.R. Howe, D.S. Klimstra, R.D. Moccia, K.C. Conlon, M.F. Brennan, Factors predictive of survival in ampullary carcinoma, Ann. Surg. 228 (1998) 87–94.
[3] K. Okano, M. Oshima, S. Yachida, Y. Kushida, K. Kato, H. Kamada, et al., Factors predicting survival and pathological subtype in patients with ampullary adenocarcinoma, J. Surg. Oncol. 110 (2014) 156–162.
[4] H. Zhou, N. Schaefer, M. Wolff, H.P. Fischer, Carcinoma of the ampulla of Vater: comparative histologic/immunohistochemical classification and follow-up, Am. J. Surg. Pathol. 28 (2004) 875–882.
[5] A. Schueneman, M. Goggins, J. Ensor, B. Saka, N. Neishaboori, S. Lee, et al., Validation of histomolecular classification utilizing histological subtype, MUC1, and CDX2 for prognostication of resected ampullary adenocarcinoma, Br. J. Cancer 113 (2015) 64–68.
[6] P. Bronsert, I. Kohler, M. Werner, F. Makowiec, S. Kuesters, J. Hoeppner, et al., Intestinal-type of differentiation predicts favourable overall survival: confirmatory clinicopathological analysis of 198 periampullary adenocarcinomas of pancreatic, biliary, ampullary and duodenal origin, BMC Cancer 13 (2013) 428.
[7] F. Yang, C. Jin, Z. Du, S. Subedi, Y. Jiang, J. Li, et al., Duodenal gastrointestinal stromal tumor: clinicopathological characteristics, surgical outcomes, long term survival and predictors for adverse outcomes, Am. J. Surg. 206 (2013) 360–367.
[8] S. Zhang, Y. Tian, Y. Chen, J. Zhang, C. Zheng, C. Wang, Clinicopathological characteristics, Surgical treatments, and survival outcomes of patients with duodenal gastrointestinal stromal tumor, Dig. Surg. (2018).
[9] P.O. Berberat, B.M. Kunzli, A. Gulbinas, T. Ramanauskas, J. Kleeff, M.W. Muller, et al., An audit of outcomes of a series of periampullary carcinomas, Eur. J. Surg. Oncol. 35 (2009) 187–191.
[10] S. Yamashita, M.J. Overman, H. Wang, J. Zhao, M. Okuno, C. Goumard, et al., Pathologic response to preoperative therapy as a novel prognosticator for ampullary and duodenal adenocarcinoma, Ann. Surg. Oncol. 24 (2017) 3954–3963.
[11] A. El Nakeeb, M. El Shobary, M. El Dosoky, A. Nabeh, M. El Sorogy, A.A. El Eneen, et al., Prognostic factors affecting survival after pancreaticoduodenectomy for pancreatic adenocarcinoma (single center experience), Hepatogastroenterology 61 (2014) 1426–1438.
[12] M. Wagner, C. Redaelli, M. Lietz, C.A. Seiler, H. Friess, M.W. Buchler, Curative resection is the single most important factor determining outcome in patients with pancreatic adenocarcinoma, Br. J. Surg. 91 (2004) 586–594.
[13] M. Zenali, M.J. Overman, A. Rashid, R.B. Broaddus, H. Wang, M.H. Katz, et al., Clinicopathologic features and prognosis of duodenal adenocarcinoma and comparison with ampullary and pancreatic ductal adenocarcinoma, Hum. Pathol. 44 (2013) 2792–2798.
[14] W. Schima, A. Ba-Ssalamah, C. Kolblinger, C. Kulinna-Cosentini, A. Puespoek, P. Gotzinger, Pancreatic adenocarcinoma, Eur. Radiol. 17 (2007) 638–649.
[15] I.T. Konstantinidis, A.L. Warshaw, J.N. Allen, L.S. Blaszkowsky, C.F. Castillo, V. Deshpande, et al., Pancreatic ductal adenocarcinoma: is there a survival difference for R1 resections versus locally advanced unresectable tumors? What is a "true" R0 resection? Ann. Surg. 257 (2013) 731–736.
[16] G. Barnes Jr., L. Romero, K.R. Hess, S.A. Curley, Primary adenocarcinoma of the duodenum: management and survival in 67 patients, Ann. Surg. Oncol. 1 (1994) 73–78.
[17] G.A. Poultsides, L.C. Huang, J.L. Cameron, R. Tuli, L. Lan, R.H. Hruban, et al., Duodenal adenocarcinoma: clinicopathologic analysis and implications for treatment, Ann. Surg. Oncol. 19 (2012) 1928–1935.
[18] M.M. Al-Hawary, R.K. Kaza, I.R. Francis, Optimal Imaging Modalities for the Diagnosis and Staging of Periampullary Masses, Surg. Oncol. Clin. N. Am. 25 (2016) 239–253.
[19] S.K. Jang, J.H. Kim, I. Joo, J.H. Jeon, K.S. Shin, J.K. Han, et al., Differential diagnosis of pancreatic cancer from other solid tumours arising from the periampullary area on MDCT, Eur. Radiol. 25 (2015) 2880–2888.
[20] A.M. Ivanovic, F. Alessandrino, R. Maksimovic, M. Micev, S. Ostojic, R.M. Gore, et al., Pathologic subtypes of ampullary adenocarcinoma: value of ampullary MDCT for noninvasive preoperative differentiation, Am. J. Roentgenol. 208 (2017) W71–W78.
[21] Y.E. Chung, M.J. Kim, M.S. Park, J.Y. Choi, H. Kim, S.K. Kim, et al., Differential features of pancreatobiliary- and intestinal-type ampullary carcinomas at MR imaging, Radiology 257 (2010) 384–393.
[22] L. Bi, Y. Dong, C. Jing, Q. Wu, J. Xiu, S. Cai, et al., Differentiation of pancreatobiliary-type from intestinal-type periampullary carcinomas using 3.0T MRI, J. Magn. Reson. Imaging 43 (2016) 877–886.
[23] B. Ganeshan, K.A. Miles, Quantifying tumour heterogeneity with CT, Cancer Imaging 13 (2013) 140–149.
[24] F. Davnall, C.S. Yip, G. Ljungqvist, M. Selmi, F. Ng, B. Sanghera, et al., Assessment of tumor heterogeneity: an emerging imaging tool for clinical practice? Insights

Imaging 3 (2012) 573–589.
[25] B. Ganeshan, K.A. Miles, S. Babikir, R. Shortman, A. Afaq, K.M. Ardeshna, et al., CT-based texture analysis potentially provides prognostic information complementary to interim fdg-pet for patients with hodgkin's and aggressive non-hodgkin's lymphomas, Eur. Radiol. 27 (2017) 1012–1020.
[26] M. Nakajo, M. Jinguji, Y. Nakabeppu, M. Nakajo, R. Higashi, Y. Fukukura, et al., Texture analysis of 18F-FDG PET/CT to predict tumour response and prognosis of patients with esophageal cancer treated by chemoradiotherapy, Eur. J. Nucl. Med. Mol. Imaging 44 (2017) 206–214.
[27] T. Hodgdon, M.D. McInnes, N. Schieda, T.A. Flood, L. Lamb, R.E. Thornhill, Can quantitative CT texture analysis be used to differentiate fat-poor renal angiomyolipoma from renal cell carcinoma on unenhanced CT images? Radiology 276 (2015) 787–796.
[28] F. Ng, R. Kozarski, B. Ganeshan, V. Goh, Assessment of tumor heterogeneity by CT texture analysis: can the largest cross-sectional area be used as an alternative to whole tumor analysis? Eur. J. Radiol. 82 (2013) 342–348.
[29] F. Ng, B. Ganeshan, R. Kozarski, K.A. Miles, V. Goh, Assessment of primary colorectal cancer heterogeneity by using whole-tumor texture analysis: contrast-enhanced CT texture as a biomarker of 5-year survival, Radiology 266 (2013) 177–184.
[30] M. Tsubakimoto, T. Yamashiro, Y. Tamashiro, S. Murayama, Quantitative CT density histogram values and standardized uptake values of FDG-PET/CT with respiratory gating can distinguish solid adenocarcinomas from squamous cell carcinomas of the lung, Eur. J. Radiol. 100 (2018) 108–115.
[31] M. Perri, P. Erba, D. Volterrani, F. Guidoccio, E. Lazzeri, D. Caramella, et al., Adrenal masses in patients with cancer: PET/CT characterization with combined CT histogram and standardized uptake value PET analysis, Am. J. Roentgenol. 197 (2011) 209–216.
[32] H.M. Namlos, K. Boye, S.J. Mishkin, T. Baroy, S. Lorenz, B. Bjerkehagen, et al., Noninvasive detection of ctDNA reveals intratumour heterogeneity and is associated with tumour burden in gastrointestinal stromal tumour, Mol. Cancer Ther. (2018).
[33] A.Y.L. Lee, C.L. Dubois, K. Sarai, S. Zarei, D.F. Schaeffer, M. Sander, et al., Cell of origin affects tumour development and phenotype in pancreatic ductal adenocarcinoma, Gut (2018).
[34] L. Gorunova, B. Johansson, S. Dawiskiba, A. Andren-Sandberg, N. Mandahl, S. Heim, et al., Cytogenetically detected clonal heterogeneity in a duodenal adenocarcinoma, Cancer Genet. Cytogenet. 82 (1995) 146–150.
[35] N. Kumari, K. Prabha, R.K. Singh, D.K. Baitha, N. Krishnani, Intestinal and pancreatobiliary differentiation in periampullary carcinoma: the role of immunohistochemistry, Hum. Pathol. 44 (2013) 2213–2219.
[36] M. Miettinen, J. Lasota, Histopathology of gastrointestinal stromal tumor, J. Surg. Oncol. 104 (2011) 865–873.
[37] C. Bai, X. Liu, C. Qiu, J. Zheng, FoxM1 is regulated by both HIF-1alpha and HIF-2alpha and contributes to gastrointestinal stromal tumor progression, Gastric Cancer (2018).
[38] L. Li, Z. Li, X. Kong, D. Xie, Z. Jia, W. Jiang, J. Cui, et al., Down-regulation of microRNA-494 via loss of SMAD4 increases FOXM1 and beta-catenin signaling in pancreatic ductal adenocarcinoma cells, Gastroenterology 147 (2014) 485–497.
[39] J. Bezy-Wendling, M. Kretowski, Y. Rolland, W. Le Bidon, Toward a better understanding of texture in vascular CT scan simulated images, IEEE Trans. Biomed. Eng. 48 (2001) 120–124.
[40] R. Takahashi, S. Tanaka, Y. Kitadai, M. Sumii, M. Yoshihara, K. Haruma, et al., Expression of vascular endothelial growth factor and angiogenesis in gastrointestinal stromal tumor of the stomach, Oncology 64 (2003) 266–274.
[41] L. Consolino, D.L. Longo, M. Sciortino, W. Dastru, S. Cabodi, G.B. Giovenzana, et al., Assessing tumor vascularization as a potential biomarker of imatinib resistance in gastrointestinal stromal tumors by dynamic contrast-enhanced magnetic resonance imaging, Gastric. Cancer 20 (2017) 629–639.
[42] Y. Yonenaga, A. Mori, H. Onodera, S. Yasuda, H. Oe, A. Fujimoto, et al., Absence of smooth muscle actin-positive pericyte coverage of tumor vessels correlates with hematogenous metastasis and prognosis of colorectal cancer patients, Oncology 69 (2005) 159–166.